

All-Optical Modulation Format Conversion and Applications in Future Photonic Networks

Ken MISHINA^{†a)}, Daisuke HISANO[†], *Members*, and Akihiro MARUTA^{†b)}, *Senior Member*

SUMMARY A number of all-optical signal processing schemes based on nonlinear optical effects have been proposed and demonstrated for use in future photonic networks. Since various modulation formats have been developed for optical communication systems, all-optical converters between different modulation formats will be a key technology to connect networks transparently and efficiently. This paper reviews our recent works on all-optical modulation format conversion technologies in order to highlight the fundamental principles and applications in variety of all-optical signal processing schemes.

key words: *optical fiber communication, all-optical signal processing, modulation format conversion, highly-nonlinear fiber, semiconductor optical amplifier*

1. Introduction

Internet traffic is increasing year-by-year, and annual global IP traffic is forecasted to reach 3.3 zettabytes by 2021 [1]. Internet communications systems will need 10-Tb/s optical interfaces working in 1-Pb/s optical transport systems by 2024 [2]. Researchers have focused on development and innovations of transmission technology that will increase the transmission capacity of optical communication systems. In the recent decade, digital coherent technology and space division multiplexing technology have innovatively increased transmission capacity. In particular, remarkable development of digital coherent technologies has greatly accelerated research on multi-level modulation formats. In backbone and metropolitan networks, conventional transmission systems based on the on-off keying (OOK) format have been gradually replaced by 100-Gb/s or 400-Gb/s transmission systems that employ quadrature-phase-shift-keying (QPSK) and quadrature amplitude modulation (QAM) formats [3], [4]. Moreover, pulse-amplitude modulation (PAM) and discrete multitone (DMT) formats using intensity modulation and direct detection (IM/DD) schemes are also expected to serve as the main modulation formats for short reach optical links such as 5G mobile fronthauls, and data center interconnects [5], [6]. The modulation format for a particular network is chosen depending on the properties of optical network, such as network size, transmission capacity, and baud rate.

On the other hand, it is essential to develop signal

processing technologies for network nodes that will support the adoption of advanced transmission technologies. All-optical signal processing is a promising technologies for the realization of elastic and power-efficient all-optical photonic networks [7]. A number of all-optical signal processing schemes have been designed to exploit nonlinear optical effects in optical fibers or semiconductor optical amplifiers (SOAs). Table 1 summarizes representative examples of all-optical signal processing schemes classified by nonlinear optical effects [7]–[22]. There are several types of nonlinear optical effect [23], [24]: self-phase modulation (SPM), cross-phase modulation (XPM), and four wave mixing (FWM) arising from third-order nonlinear susceptibility $\chi^{(3)}$ in optical fibers or a change of carrier density in SOAs. Cross-gain modulation (XGM) is also caused in SOA. Phonon oscillation in optical fibers leads to stimulated Raman scattering (SRS) and stimulated Brillouin scattering (SBS). Optical solitons, supercontinuum (SC) generation, and parametric amplification (PA) can be understood as by-products of $\chi^{(3)}$ nonlinear effects in optical fibers. When using these nonlinear optical effects for signal processing, nonlinearities must be induced selectively and efficiently, and unwanted nonlinear effects must be suppressed.

For all-optical signal processing, a range of advanced

Table 1 All-optical signal processing schemes classified by nonlinear optical effects [7]–[22].

Nonlinear effect	Signal processing scheme
SPM	Regeneration (Fiber, SOA)
XPM	Wavelength conversion (Fiber, SOA) Regeneration (Fiber, SOA) A/D conversion (Fiber) Multiplexing/demultiplexing (Fiber) Modulation format conversion (Fiber, SOA) Logical gate (Fiber, SOA) Tunable delay line (Fiber)
FWM	Wavelength conversion (Fiber, SOA) Regeneration (Fiber) Multiplexing/demultiplexing (Fiber) Optical conjugation (Fiber)
XGM	Wavelength conversion (SOA) Synchronization detection (SOA)
SRS	Tunable delay line (Fiber)
SBS	Tunable delay line (Fiber)
Soliton	A/D conversion (Fiber) Bit rate conversion (Fiber)
SC	A/D conversion (Fiber)
PA	A/D conversion (Fiber) Modulation format conversion (Fiber) Tunable delay line (Fiber)

Manuscript received July 31, 2018.

Manuscript revised November 21, 2018.

[†]The authors are with Osaka University, Suita-shi, 565–0871 Japan.

a) E-mail: mishina@comm.eng.osaka-u.ac.jp

b) E-mail: maruta@comm.eng.osaka-u.ac.jp

DOI: 10.1587/transele.2018ODI0002

Table 2 Comparison between HNLF and SOA.

	HNLF	SOA
Response time	Several fs	Several dozen ps Several ps (QD-SOA)
Device length	0.1 - 10 km	100 - 2,000 μm
Photonics integration	N/A	Available
Device type	Passive	Active
Amplification	N/A	Available
Noise figure	N/A	5 dB
Power consumption	N/A	Several hundred mW
Required optical power for signal processing	10 - 30 dBm	0 - 20 dBm

devices and materials has been studied, such as silicon waveguides [25], periodically poled lithium niobate (PPLN) waveguides [26], and photonic crystals [27]. We concentrate on highly nonlinear fiber (HNLF) and SOA as nonlinear optical devices in this paper because they are used most widely. The relevant properties HNLF and SOA are summarized in Table 2. HNLF offers a better response time. On the other hand, SOA offers better photonics integration and device compactness. Although conventional SOA has had limitations of operation speed, the response time has significantly improved by development of quantum dot (QD)-devices [28].

In this paper, we focus on all-optical modulation format conversion, which will be essential for connecting the different kinds of modulation format transparently. Our recent studies on conversions from OOK to binary phase shift keying (BPSK) and multi-level modulation format are reviewed below to explain the fundamental principles and design of the modulation format converter. In Sect. 2, we introduce the basic principle of the modulation format conversion from OOK to BPSK based on XPM, which is the most basic functional block in a modulation format converter. In Sect. 3, we describe how to design high-performance OOK to multi-level modulation format converter, and we introduce examples of several converters. Section 4 presents the advanced applications in which modulation format converters can be used for photonic networks. Finally, Sect. 5 concludes the discussion.

2. Basic Principle of Modulation Format Conversion

In this section, we introduce the principles of OOK/BPSK modulation format converters, which are the most basic functional blocks. XPM can be used to convert amplitude modulation to phase modulation, and the detailed mechanisms of this conversion are explained below.

2.1 SOA-Based OOK/BPSK Format Converter

Figure 1 (a) shows a schematic diagram of OOK/BPSK format conversion using Mach-Zehnder interferometer (MZI) as an SOA [14]. The basic configuration is almost the same as that of the conventional SOA-MZI wavelength converter [29], except for the level of the bias current at each SOA: the bias current of SOA#2, which is used as an output

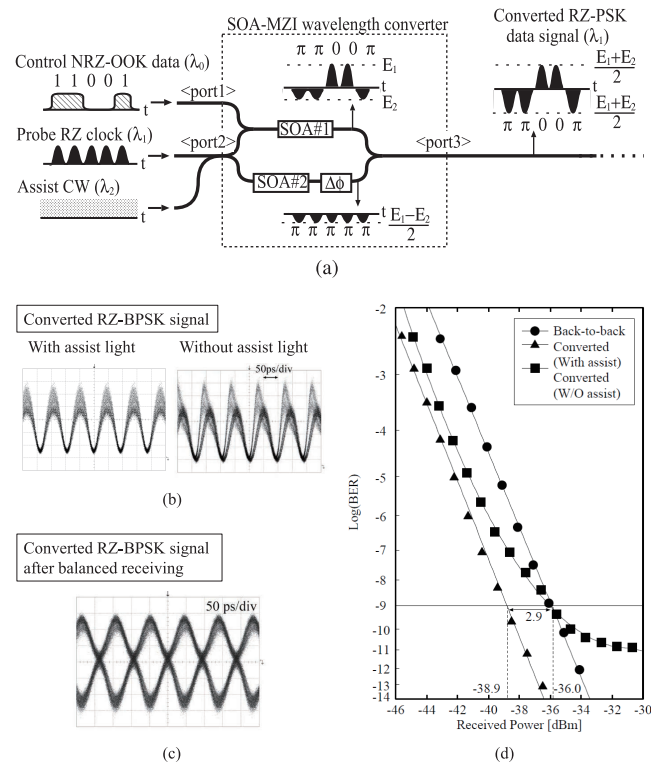


Fig. 1 OOK/BPSK format conversion based on SOA-MZI: (a) schematic diagram, (b) eye diagrams of converted RZ-BPSK signals with and without assist light, (c) eye diagram after the balanced receiver, and (d) measured BER.

power adjuster, is considerably lower than that of SOA#1. Non-return-to-zero (NRZ)-OOK signal pulses at a wavelength of λ_0 are launched into the upper arm of the MZI as control pulses. A return-to-zero (RZ)-clock pulse sequence at λ_1 and continuous wave (CW) light at λ_2 are launched into both arms of the MZI as probe pulses and as assist light, respectively. In SOA#1, the carrier density is varied according to the amplitude of the control pulse, and the phase and amplitude of the probe pulse are changed after passing through SOA#1 because of XPM and XGM, respectively. E_1 and E_2 are the amplitudes of the probe pulse after passing through SOA#1 with no control pulse (corresponding to logical “0”) and with a control pulse (corresponding to “1”), respectively. The current levels of SOA#2 and the SOA-based phase shifter are adjusted so that the probe pulse takes an overall phase-shift of “ π ” and amplitude of $(E_1 - E_2)/2$ on the lower arm. Without a control pulse, the probe pulse has the phase of “0” and the amplitude of E_1 after passing through SOA#1, and the phase and amplitude of the converted signal observed at the output of SOA-MZI are, respectively, “0” and $(E_1 + E_2)/2$ because of the anti-phase interference. When the control pulse is present, the probe pulse has the phase of “ π ” and amplitude of E_2 after passing through SOA#1. The phase and amplitude of the converted signal observed at the output of the SOA-MZI are, respectively, “ π ” and $(E_1 + E_2)/2$ because of the in-phase interference. Thus, the NRZ-OOK data signal can be converted to

an RZ-BPSK data signal. The assist light is launched to suppress the rapid change of carriers, which induces frequency chirp and amplitude fluctuation.

The proposed OOK/BPSK conversion was demonstrated experimentally with a monolithically integrated SOA-MZI and 10.7 Gb/s pseudorandom binary sequence (PRBS) of length $2^{31} - 1$. Figure 1 (b) shows eye diagrams for a 10.7 Gb/s converted signal with and without the assist light. With assist light, an RZ pulse train was clearly observed. On the other hand, we observed overshooting at the leading edge of the pulse without assist light because of pattern effect. A clear eye opening appears after the balanced receiver in Fig. 1 (c). Figure 1 (d) shows the obtained bit-error rate (BER) of the converted signal with and without assist light. We can see that an error-free operation was achieved with the assist light. The received sensitivity of the converted signal with assist light is improved by 2.9 dB at BER of 10^{-9} because of the balanced detection, which suggests that there is no power penalty due to the conversion. The above mentioned results reveal that the NRZ-OOK signal can be converted into an RZ-BPSK signal with using SOA-MZI. Furthermore, the suitable dispersion tolerance of a converted RZ-BPSK signal for long-haul transmission up to ± 500 ps/nm has been reported [14].

The phase change of the probe pulse because of XPM is caused by the change of the carrier density in SOA. When analyzing an SOA, the SOA is generally divided into multiple sections and the following rate equation for the carrier density [30] is used, considering the fields in each section:

$$\frac{dN_i}{dt} = \frac{J}{qd} - \frac{N_i}{\tau_i} - \sum_{x=c,p,a} \frac{g_m^{(x)} \cdot I_i^{(x)}}{E^{(x)}} - g_m^{(ASE)} S_i, \quad (1)$$

where N is the carrier density, J is the injection current density, d is the active layer thickness, τ is the carrier lifetime, g_m is the material gain, I is the injected light intensity, E is the photon energy, and S_i is the average amplified spontaneous emission (ASE). Subscript i indicates the different sections and superscript x ($= c, p$, and a) denotes the control, probe and assist light, respectively. The nonlinear phase change $\Delta\phi_i$, arising from carrier density-induced changes in the refractive index, is given by [24]

$$\Delta\phi_i = \frac{\pi\Delta L\Gamma g_{m_i}}{2a_1\lambda} \Delta\bar{n}_N. \quad (2)$$

The parameter ΔL is the cavity length of a divided section, Γ is the confinement factor, and $\Delta\bar{n}_N$ is the rate of change of the refractive index in the active region concentrated carriers. The material gain g_{m_i} is proportional to the carrier density N_i and all other parameters are constants. Therefore, the nonlinear phase change in the SOA is proportional to the sum of the carrier-density changes in the divided sections. In the case of our proposed OOK/BPSK converter, the phase of the RZ pulse train is changed affected by the carrier-density changes arising from the NRZ-OOK signal input. The nonlinear gain change, namely XGM, is also caused by carrier density changes. The optical gain G_i of section i is given by

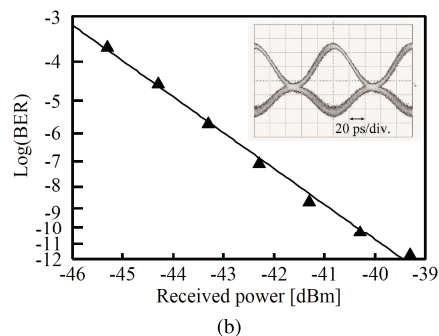
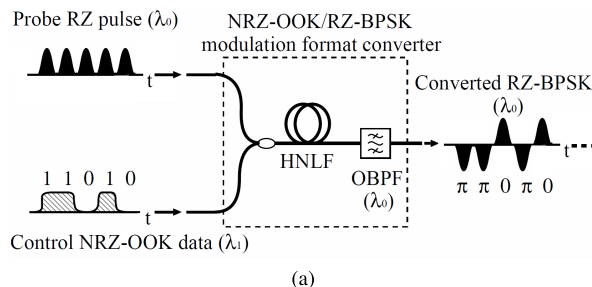


Fig. 2 OOK/BPSK modulation format conversion based on HNLf: (a) schematic diagram and (b) measured BER and eye diagram after the balanced receiver.

$$G_i = \exp \{g_{m_i}(N_i) \cdot \Delta L\}. \quad (3)$$

The total gain through SOA is product of optical gains of all sections. The gain of the RZ pulse train is also changed affected by the NRZ-OOK signal input. Therefore, output power will need to be adjusted when we use SOA for OOK/BPSK modulation format conversion.

2.2 HNLf-Based OOK/BPSK Format Converter

Figure 2 (a) shows a schematic diagram of OOK/BPSK format conversion using HNLf [13]. An RZ pulse sequence and an NRZ-OOK signal are synchronously launched into the HNLf as a probe pulse and a control pulse, respectively. The phase of the probe pulse is modulated by XPM that is driven by the control pulses.

XPM is induced by variation in the the refractive index Δn_{NL} , which is associated with the third-order nonlinear susceptibility $\chi^{(3)}$ [23]. Δn_{NL} is given by

$$\Delta n_{NL} = \frac{n_2}{A_{\text{eff}}} (P^{(p)} + 2P^{(c)}), \quad (4)$$

where n_2 is the nonlinear refractive index, A_{eff} is the effective mode area, and $P^{(x)}$ is the optical power. Superscripts x (c and p) distinguish between the control and probe pulses. The variation in the fiber's propagation constant β , namely, $\Delta\beta$, is proportional to Δn_{NL} such that

$$\Delta\beta = k_0 \Delta n_{NL} = \gamma (P^{(p)} + 2P^{(c)}). \quad (5)$$

Here, $k_0 = 2\pi/\lambda$ is the wave number in a vacuum, and $\gamma = k_0 n_2 / A_{\text{eff}}$ is the nonlinear coefficient of the optical fiber. Since the optical phase shift increases linearly with distance

z , the nonlinear phase shift ϕ_{NL} is given by

$$\begin{aligned}\phi_{\text{NL}} &= \int_0^L \Delta\beta dz \\ &= \int_0^L \gamma \{P^{(p)}(z) + 2P^{(c)}(z)\} dz \\ &= \gamma L_{\text{eff}}(P_{\text{in}}^{(p)} + 2P_{\text{in}}^{(c)}),\end{aligned}\quad (6)$$

where $P^{(x)}(z) = P_{\text{in}}^{(x)} \exp(-\alpha z)$ accounts for the fiber loss α , and L_{eff} is the effective interaction length of the HNLF. Therefore, the phase change of the probe pulse due to XPM $\Delta\phi$, is described by

$$\Delta\phi = 2\gamma L_{\text{eff}} P_{\text{in}}^{(c)}.\quad (7)$$

Equation (7) shows that the phase change of the probe pulse is proportional to the peak input power of the control pulse. The peak power of the control pulse is adjusted so that the phase change of the probe pulse affected by the control pulse $\Delta\phi$ becomes “ π ”. After passing through the HNLF, the probe pulse has two different phases, “0” or “ π ”, depending on the control pulse signal. Therefore, an NRZ-OOK signal can be converted to an RZ-BPSK signal. 10 Gb/s error-free operation with a clear eye opening was has been demonstrated experimentally, as shown in Fig. 2 (b).

Other methods for OOK/BPSK conversion using XPM in a single SOA have been proposed [31], including nonlinear optical loop mirrors (NOLMs) [32], silicon microring resonators [33], and passive waveguides [34].

3. Conversion to Multi-Level Modulation Format

Generally speaking, a highly functional system can be designed by combining basic functional blocks in series or parallel. Figure 3 (a) illustrates the basic concept of the serial configuration. The relation between the input and output optical electric fields of the functional blocks, $E_{\text{in}}^{(A)}$, $E_{\text{in}}^{(B)}$ and E_{out} , is expressed as

$$E_{\text{out}} = f_B(f_A(E_{\text{in}}^{(A)}), E_{\text{in}}^{(B)}),\quad (8)$$

where $f_A(E_1)$ and $f_B(E_1, E_2)$ represent the input-output

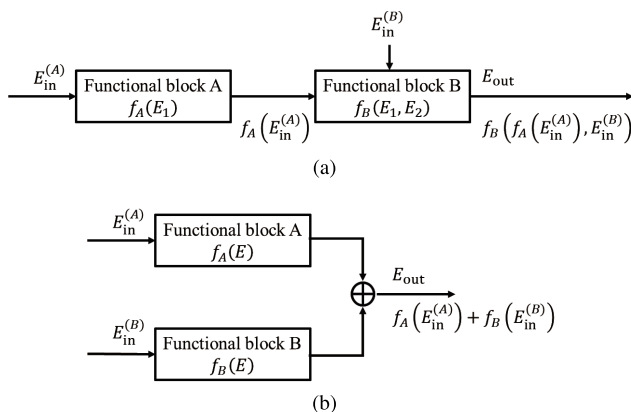


Fig. 3 Concepts of (a) serial and (b) parallel configurations.

functions of functional blocks A and B, respectively. Equation (8) indicates that the serial configuration can express the composition of functions A and B.

Figure 3 (b) shows the general concept of the parallel configuration of functional blocks. The relation between the input and output optical electric fields of the functional blocks is expressed as

$$E_{\text{out}} = f_A(E_{\text{in}}^{(A)}) + f_B(E_{\text{in}}^{(B)}).\quad (9)$$

Equation (9) indicates that the parallel configuration sums up the output electrical fields of the functional blocks.

Figure 4 illustrates examples of the serial configuration, for an OOK/QPSK converter and an OOK/4 amplitude and phase shift keying (APSK) converter. The OOK/QPSK converter is constructed with an OOK/BPSK converter and an $\pi/2$ phase modulator serving as functional blocks A and B, respectively. In this arrangement, the converted QPSK signal is not a gray code. An OOK/4APSK converter can be realized by implementing an OOK/BPSK converter and an amplitude modulator as functional blocks A and B, respectively. The serial configuration is suitable if functional blocks A and B are different. By connecting more functional blocks in series, M-ary PSK and APSK signals can be generated.

Figure 5 shows examples of the parallel configuration of functional blocks. OOK/QPSK (4QAM) converters and OOK/16QAM converters can be designed with two OOK/BPSK converters and two OOK/QPSK converters configured in parallel as functional blocks A and B, respectively. The electric field output is determined by the interference of the electric field output from functional blocks A and B. The QPSK signal is generated by orthogonal multiplexing of two BPSK signals. The 16QAM signal can be obtained by multiplexing two QPSK signals with small and large amplitudes. As shown in the above examples, the parallel configuration is suitable for converters in which

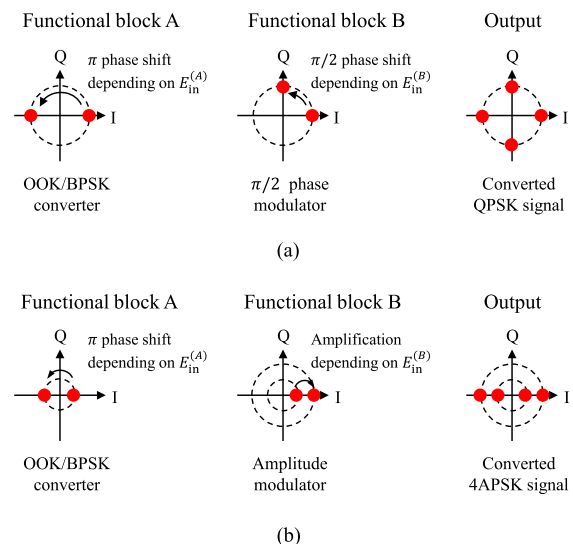


Fig. 4 Examples of serial configurations for the (a) OOK/QPSK converter and (b) OOK/4APSK converter.

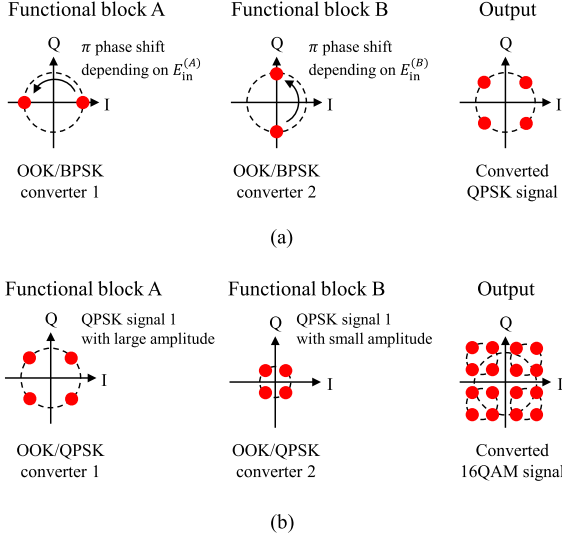


Fig. 5 Examples of parallel configurations for the (a) OOK/QPSK converter and (b) OOK/16QAM converter.

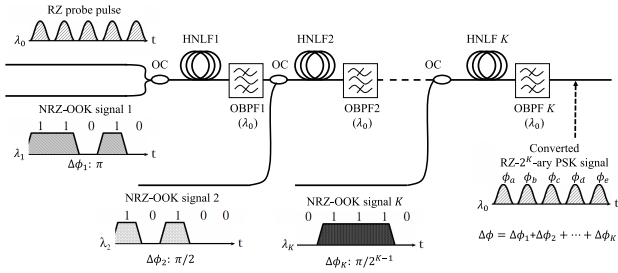


Fig. 6 OOK/M-ary PSK modulation format converter based on HNLFs.

functional blocks A and B have the same function like the two OOK/BPSK converters shown in Fig. 5 (a). By configuring more functional blocks in parallel, a 2^M -QAM signal can be composed from M channels of OOK signals.

Next, we introduce several examples of converters that change multi-channel OOK signals to multi-level modulation formats: M -ary PSK, APSK, and QAM.

3.1 Serial Configuration

3.1.1 OOK to M -ary PSK Conversion

Figure 6 shows the schematic diagram of the OOK/ M -ary PSK modulation format converter based on serial-connected HNLFs. The channel k NRZ-OOK signal is launched into each k -th HNLF as control pulse k . In this scheme, the phase change of the output probe pulse because of XPM $\Delta\phi$ is described by

$$\Delta\phi = \sum_{k=1}^K \Delta\phi^{(k)} = 2 \sum_{k=1}^K \gamma^{(k)} L_{\text{eff}}^{(k)} P_{\text{in}}^{(k)}, \quad (10)$$

where $\Delta\phi^{(k)}$ is the phase change of the probe pulse that is induced by control pulse k . $\gamma^{(k)}$ and $L_{\text{eff}}^{(k)}$ are the nonlinear coefficient and the effective interaction length of HNLF k

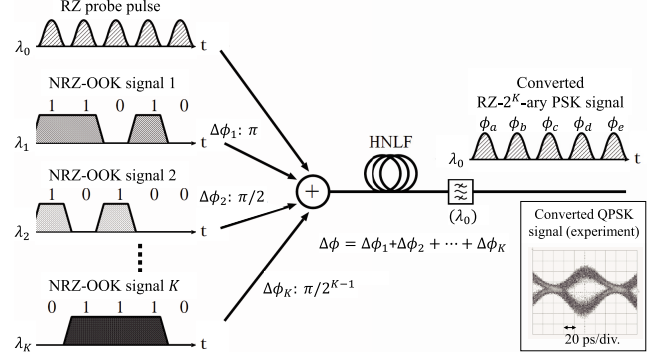


Fig. 7 Another OOK/ M -ary PSK modulation format converter based on HNLFs.

respectively. The peak power of control pulse k (P_k) is adjusted so that the probe pulse phase change induced by control pulse k ($\Delta\phi_k$) is kept at $\pi/2^{k-1}$. After passing through all HNLFs, the probe pulse has 2^K different phases, depending on the combination of control pulses. Therefore, NRZ-OOK signals can be converted to RZ- 2^K -ary PSK signal. When K is 1, 2 and 3, the converted signals are RZ-BPSK, RZ-QPSK and RZ-8PSK signals, respectively. The same wavelength for all NRZ-OOK signals from 1 to K ($\lambda_0 = \lambda_1 = \dots = \lambda_K$) is available because the NRZ-OOK signals are separated by optical band-pass filters (OBPFs). However, this modulation format converter requires many optical components, including many HNLFs and OBPFs. Therefore, we have proposed another design for OOK/ M -ary PSK modulation format conversion that only uses an HNLF. The proposed design is illustrated in Fig. 7 [13]. In this scheme, parallel K -channels of NRZ-OOK signals are launched simultaneously into an HNLF as control pulses. The phase change of the probe pulse caused by XPM $\Delta\phi$ is represented by

$$\Delta\phi = \sum_{k=1}^K \Delta\phi^{(k)} = 2\gamma L_{\text{eff}} \sum_{k=1}^K P_{\text{in}}^{(k)}. \quad (11)$$

Equation (11) indicates that the phase change of the probe pulse is proportional to the summation of the peak power of K control pulses. After passing through the HNLF, the probe pulse has 2^K different phases. The parameters of the HNLF limit the possible number of modulated phases in the converted signal because of FWM and walk-off between probe pulse and control pulses. We have reported a design method of wavelength allocation of input OOK signals in [35].

A more advanced PAM4 to QPSK modulation format converter, based on the design of an OOK/QPSK converter using HNLFs, has also been reported [36].

3.1.2 OOK to APSK Conversion

APSK is a modulation format that combines ASK and PSK. The OOK/APSK modulation format converter is built from functional blocks for phase and amplitude modulation. Figure 8 shows the schematic diagram for OOK/8APSK con-

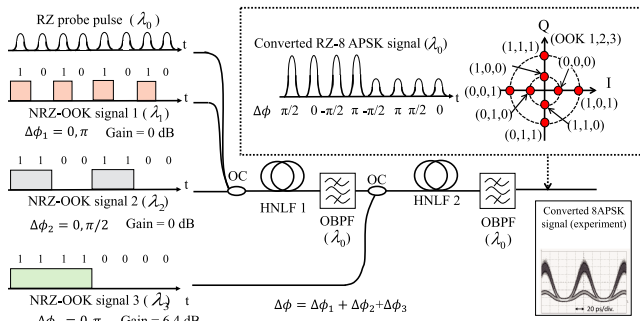


Fig. 8 OOK/8APSK modulation format converter based on HNLF.

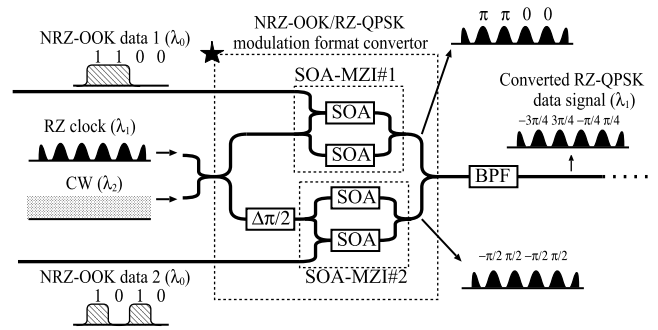
version [22]. In HNLF 1, a probe pulse is modulated to the QPSK format using the OOK/QPSK converter based on HNLF as described in 3.1.1. The converted QPSK signal after passing through HNLF 1 and NRZ-OOK signal 3 are launched into the HNLF 2 simultaneously. In HNLF 2, the converted QPSK signal is converted to 8APSK format via PA in HNLF 2. In our experience, the parameters of the HNLF 2 and NRZ-OOK 3 signals were chosen so that the peak power of the converted QPSK signal can be amplified effectively by co-propagation with the NRZ-OOK 3 pulse. In concrete term, parameters should be chosen so that the dispersion parameter of HNLF 2 is close to “0” and wavelengths of the QPSK and the NRZ-OOK 3 signals are similar, in order to decrease the difference in the propagation constants of the QPSK and NRZ-OOK 3 signals.

As another example, another lab has demonstrated an all-optical modulation format converter from ASK and QPSK to 8QAM using the FWM effect in HNLF [37].

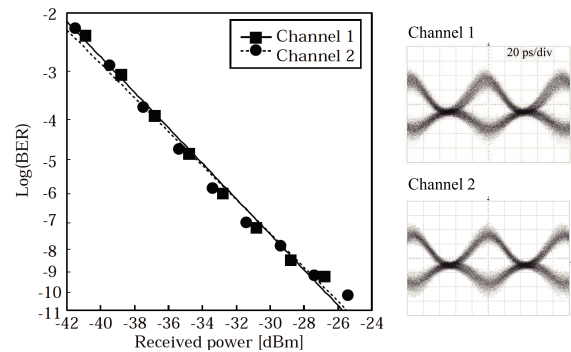
3.2 Parallel Configuration

3.2.1 OOK to QPSK Conversion

Figure 9(a) shows a schematic diagram of the OOK/QPSK modulation format converter that uses parallel SOA-MZIs [38]. The basic configuration consists of an SOA-MZI OOK/BPSK modulation format converter (SOA-MZI#1) on the upper arm and another SOA-MZI#2 with a phase shifter connected in tandem on the lower arm. NRZ-OOK data signals 1 and 2 with a wavelength of λ_0 are launched into the upper arm of the MZI (port 1) and the lower arm of the MZI (port 3), to serve as control pulses 1 and 2, respectively. An RZ-clock pulse sequence with wavelength λ_1 is launched into the MZI (port 2) as a probe pulse. According to the NRZ-OOK data “1” or “0”, the phase of the probe pulse after it passes through SOA-MZI#1 shifts by either “0” or “ π ”. On the other hand, when data signal 2 is either “0” or “1”, the probe pulse has a phase of “ $\pi/2$ ” or “ $-\pi/2$ ” after passing through the SOA-MZI#2 because of the $\pi/2$ phase shifter. After passing through SOA-MZI#1 and #2, the probe pulses have equal peak power and cause orthogonal interference in each combination of control pulses 1 and 2. The probe pulse at the output has the same peak amplitude as the incoming signals because of this orthogonal interference and



(a)



(b)

Fig. 9 OOK/QPSK modulation format conversion using parallel SOA-MZIs: (a) schematic diagram and (b) measured BER and eye diagrams of both channels 1 and 2 of the balanced receiver.

has four different phases depending on the combination of control pulses 1 and 2. This process converts NRZ-OOK data signals into RZ-QPSK data signals. A 20 Gb/s error-free operation with clear eye openings in both channels 1 and 2 was also experimentally demonstrated as shown in Fig. 9(b). Channel 1 and 2 are the outputs of the 1-bit delay interferometer with $\Delta\pi/4$ and $-\Delta\pi/4$ phase shifters at the differential QPSK receiver. We reported a reasonable dispersion tolerance up to ± 295 ps/nm in the converted RZ-QPSK signal [38]. High-speed QPSK signal generation using photonic-integrated parallel SOA-MZIs at a bit rate of 173 Gb/s has also been demonstrated by another research group [39].

Another example of all-optical BPSK/QPSK conversion using a conventional delay-line interferometer has been studied [40]. In this scheme, the input BPSK signal is demultiplexed into a pair of BPSK signals. Then, the two BPSK signals are combined by a delay interferometer and converted into a QPSK signal.

3.2.2 OOK to 16QAM Conversion

Figure 10(a) shows a schematic diagram of the OOK/16QAM modulation format converter with parallel SOA-MZIs [41]. The basic configuration consists of an SOA-MZI NRZ-OOK/RZ-QPSK format converter (#1) on the upper arm and another NRZ-OOK/RZ-QPSK format converter (#2) on the lower arm. The upper-arm RZ-QPSK signal is generated by orthogonal interference between the two

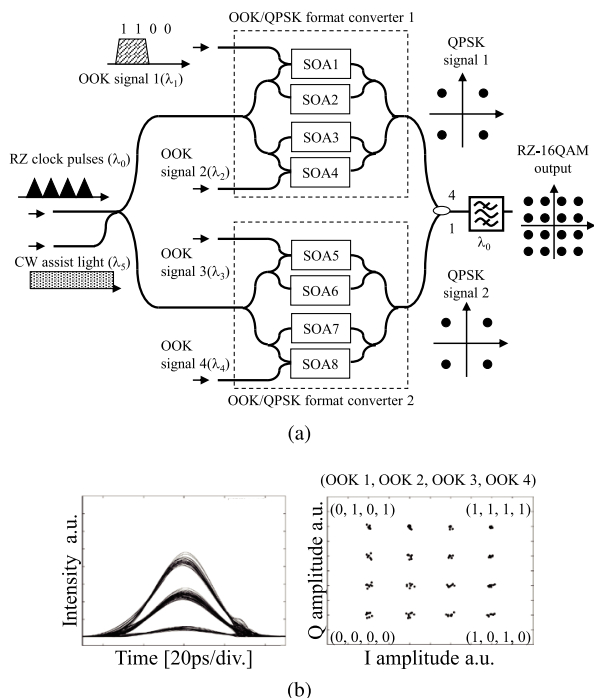


Fig. 10 OOK/16QAM modulation format conversion using parallel SOA-MZIs: (a) schematic diagram and (b) calculated eye diagram and constellation map of the converted RZ-16QAM signal.

RZ-BPSK signals. In the OOK/16QAM format converter on the lower arm, NRZ-OOK signals 3 and 4 are converted to a second RZ-QPSK signal. Finally, the RZ-16QAM signal is generated by coupling the two RZ-QPSK signals at a 4 : 1 power ratio [43]. Figure 10(b) shows our simulation results in the form of the calculated eye diagram and a constellation map of the converted 16QAM signal. A clear eye opening and a well-defined 16QAM constellation map were observed at a bit rate of 40 Gb/s. This method has the disadvantage that the required number of SOA is increased by the number of multi-level signals involved. Another method for OOK/16QAM conversion that uses only 5 SOAs has been proposed [42]. Integration with photonic components and the experimental demonstration of this designs performance have not yet been reported.

Figure 11 shows the configuration of an OOK/16QAM modulation format converter that consists of a NOLM with a 1 : 2 coupler [44]. We mark the four ports of the 1 : 2 as couplers 1, 2, 3, and 4, as shown in Fig. 11. This converter has a 1 : 2 power-splitting ratio, and the phases of the coupled output signal and the through-output signal are separated by 90°. Port 3 serves as the input port. When a probe pulse is launched into the NOLM through the coupler, it will be split into two pulses from ports 1 and 2. These split probe pulses travel through the loop clockwise and counter-clockwise. The clockwise OOK signals 1 and 2 are used to modulate the probe pulse into QPSK 1 via XPM in the HNLF, as shown in Fig. 11. On the other hand, the counter-clockwise OOK signals 3 and 4 are used to modulate QPSK 2. The nonlinear phase changes of the clockwise and counter-clockwise

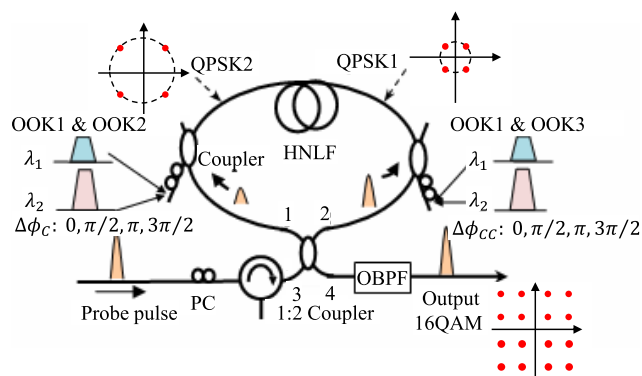


Fig. 11 OOK/16QAM modulation format converter based on NOLM.

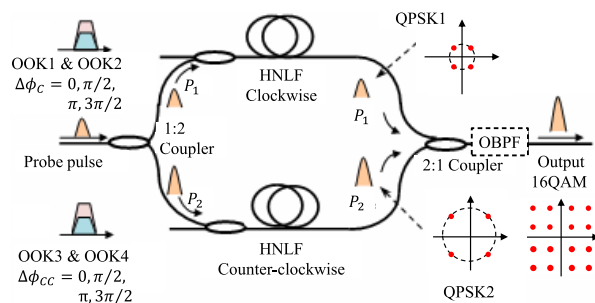


Fig. 12 MZI configuration of the OOK/16QAM modulation format converter based on HNLF.

probe pulses, $\Delta\phi_C$ and $\Delta\phi_{CC}$, are induced by XPM between the co-propagating OOK signals. They are described with the following equations:

$$\Delta\phi_C = 2\gamma L_{\text{eff}}(P_{\text{OOK1}} + P_{\text{OOK2}}), \quad (12)$$

$$\Delta\phi_{CC} = 2\gamma L_{\text{eff}}(P_{\text{OOK3}} + P_{\text{OOK4}}), \quad (13)$$

where $P_{\text{OOK}i}$ denotes the peak powers of the OOK i signals. The peak powers of the OOK i signals are adjusted with OOK/QPSK converter that was described in 3.1.1. The clockwise and counter-clockwise probe pulses are converted to QPSK 1 and QPSK 2 signals, respectively. Therefore, the output signal is the superposition of two QPSK signals at a power ratio of 1 : 2. Finally, the converted 16QAM signal is generated at the output of the converter.

This NOLM configuration of the OOK/16QAM converter can be replaced by the MZI configuration shown in Fig. 12. The probe pulses, divided into the upper and lower branches of the MZI, correspond to the clockwise and counter-clockwise probe pulses in the NOLM. This correspondence is related to how the OOK/16QAM modulation format converter is constructed by arranging two OOK/QPSK converters in parallel. However, the properties of the HNLFs in the upper and lower MZI branches must be identical. Since it is difficult to prepare two HNLFs with identical lengths, nonlinear coefficients, and losses, the NOLM configuration is more suitable for realizing an OOK/16QAM modulation format converter. Numerical and experimental demonstrations of this arrangement have also been reported [44], [45]. However, the output 16QAM

Table 3 Comparison of all-optical modulation format converters.

Device	SOA		HNLF	
	Single SOA	SOA-MZI	Simple HNLF	NOLM
Demonstrated format conversion	OOK/BPSK	OOK/BPSK OOK/QPSK OOK/16QAM	OOK/BPSK OOK/QPSK OOK/8PSK	OOK/BPSK OOK/16QAM
Symbol rate (GSymbol/s)*	8	10	40	40
Power penalty (dB)*	3.0	0.1	0.9	No data
Total input optical power (mW)*	1.6	25.1	41.9	80.4
Power for driving device (mW)*	No data	700-800	Unnecessary	Unnecessary
Optical integration	Available	Available	N/A	N/A
Device length*	No data	1,800 μm (SOA)	2.4 km	380 m (HNLF)
Reference	[31]	[14], [38], [41]	[13], [22]	[32], [44], [45]

*Representative values for OOK/BPSK conversion

signals are particularly affected by ASE noise in the amplified OOK signals, and this issue needs to be addressed in further research.

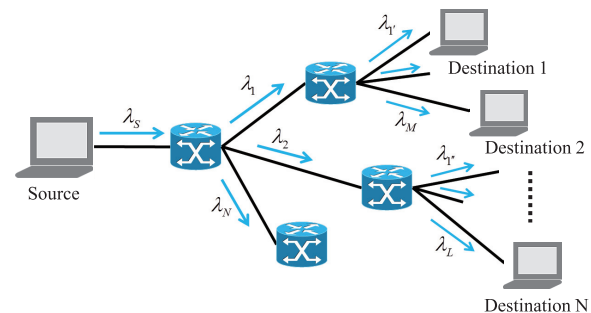
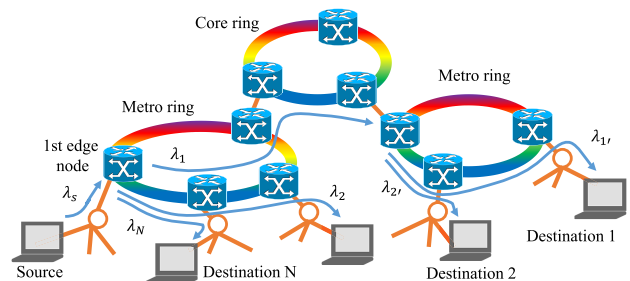
3.3 Performance of Modulation Format Converter

Table 3 shows a comparison of the all-optical modulation format converters introduced above. SOA-based converters have the advantages of low optical input power and small size because SOA offers high gain and high nonlinear coefficients. The main technical limitation of SOA-based converters is operation speed, as evidenced by the 25 GSymbol/s QPSK and 16QAM transmission systems that have already been deployed for practical use [3], [4]. Owing to recent developments of SOA components with QD technology, high-speed operation over 40 GSymbol/s using photonic-integrated parallel MZIs has been reported [39]. SOA-based modulation format converters are therefore suitable for application to optical communication systems presently in use.

HNLF-based converters are superior in operation speed. Symbol rates over 80 or 160 GSymbol/s are possible because the response time of $\chi^{(3)}$ nonlinear effects is several femtoseconds. Therefore, HNLF-based converters are suitable for use in future high-speed photonic networks. The main technical problems with HNLF-based converters are the long device size and high-optical-power operation because the nonlinear effects in the fibers come at a great cost to efficiency. To further improve these devices, development of silicon waveguides [25] and photonic crystals [27], will be needed as substitutes for HNLF materials to increase the nonlinear coefficient. Conversion to the multi-level format of 16QAM, which is the largest number of multi-level signals in current practical use, can be realized using parallel configurations based on either SOA or HNLF components.

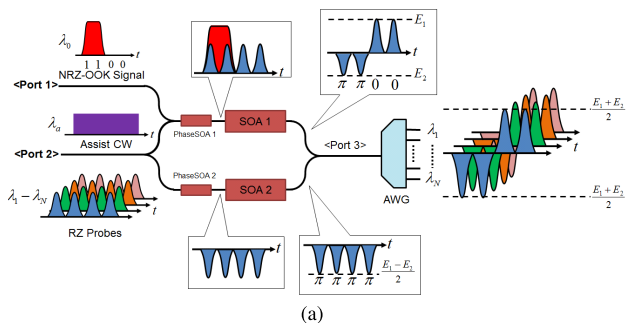
4. Application in Future Photonic Networks

All-optical modulation format converters can also be used for other applications in future photonic networks. This section explains those applications and how the nonlinear modulation format converter is useful for them.

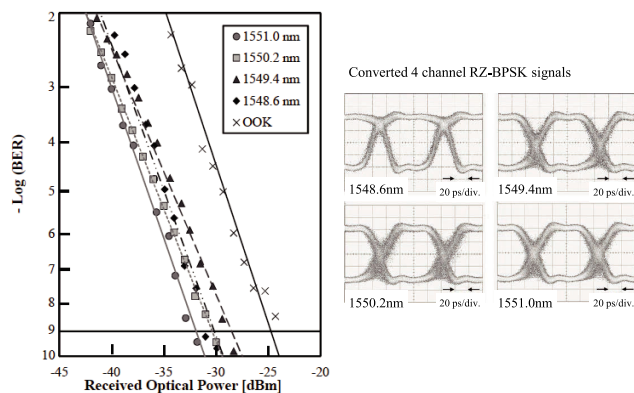
**Fig. 13** Concept of a WDM multicasting system.**Fig. 14** Example of a WDM multicasting system in future photonic networks.

4.1 WDM Multicasting

Figure 13 shows a schematic diagram of the data flow in a wavelength division multiplexing (WDM) multicast network. The communication network has been evolved from point-to-point transmission to point-to-multi-point transmission. The demand for this technology has been strengthened by increasing popularity of the streaming television, video-conferencing, and the like. The point-to-multi-point network structure can drastically reduce traffic capacity. Optical layer multicasting has been studied, and several all-optical wavelength-multicasting schemes have been proposed [46], [47] to meet the increasing demand for widely distributed Internet traffic. For the example of the WDM multicasting system illustrated in Fig. 14, the all-optical OOK/BPSK modulation format converter holds promise for use at the first edge node in future photonic networks if OOK



(a)



(b)

Fig. 15 Wavelength-multicasting accompanied with OOK/BPSK converters based on SOA-MZI: (a) schematic diagram and (b) measured BER and eye diagrams of converted four-channel RZ-BPSK signals after balanced receiving.

and BPSK formats have been adopted for access network and metro-ring network, respectively.

We introduce the wavelength-multicasting schemes accompanied with all-optical OOK/BPSK modulation format converters described in Sect. 2. Figure 15(a) shows a schematic diagram of an all-optical wavelength-multicasting scheme using SOA-MZI OOK/BPSK converters [48]. An NRZ-OOK signal pulse with a wavelength of λ_0 is launched into the upper arm of the MZI as a control pulse. Multi-wavelength RZ pulse sequences with $\lambda_1 - \lambda_N$ are launched into both arms of the MZI as N probe pulses. The phases of all RZ pulse sequences with $\lambda_1 - \lambda_N$ are then changed depending on the presence or absence of the NRZ-OOK signal. The phase modulated RZ pulse sequences with $\lambda_1 - \lambda_N$ are analyzed in each wavelength channel by an arrayed waveguide grating (AWG). Finally, the NRZ-OOK signal pulse at λ_0 is converted to RZ-BPSK signals at wavelengths of $\lambda_1 - \lambda_N$. Figure 15(b) shows the experimental data that confirm the system's error-free operation for four-channel multicasting at a bit rate of 10 Gb/s.

Figure 16 shows another wavelength-multicasting method based on HNLf components [49]. In the same way as that of SOA-based multicasting, N -channel BPSK signals can be generated using HNLf-based OOK/BPSK converters. Note here that the number of channels is mainly limited by the effects of FWM and walk-off due to fiber

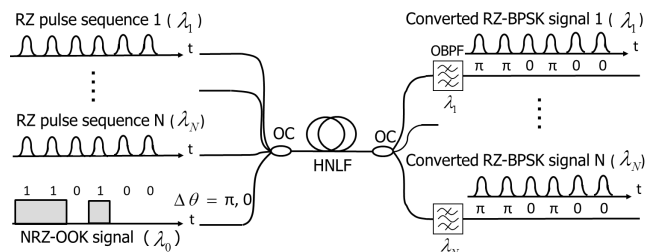


Fig. 16 Wavelength multicasting accompanied with OOK/BPSK converter based on HNLf.

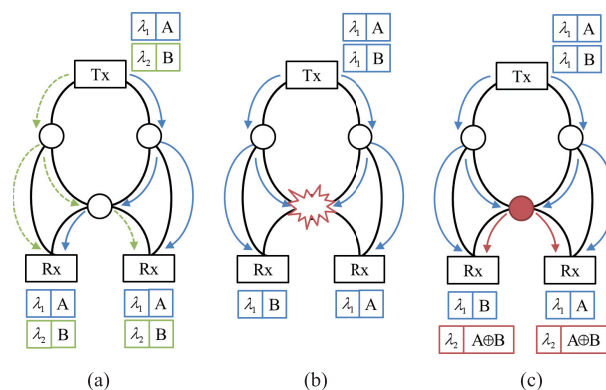


Fig. 17 Example of optical multicasting and network coding: (a) normal optical multicasting, (b) collision case, (c) network coding.

dispersion. For example, the difference in wavelengths between the NRZ-OOK signal and RZ pulse sequence should be over 7 nm in order to avoid unexpected PA in the case of the HNLf material that we tested. We assume that the operation bandwidth is limited to the C-band (1530–1565 nm) by the bandwidth of the erbium-doped fiber amplifier (EDFA) material. The RZ pulse sequence should be allocated in the remaining 28 nm of the bandwidth within the C-band. In this case, the maximum number of multicasting wavelength channels is limited to 35 when the wavelength interval is 0.8 nm (100 GHz). Moreover, a power penalty occurs is likely to arise because of walk-off at the outermost wavelength channel.

4.2 Network Coding

In optical multicasting communication systems, the optical signal is branched by an optical splitter in relay node, and the optical signal is then forwarded to multiple paths as required. This arrangement offers the advantage that the transmitted optical signal is not converted to an electrical signal so that it is not limited by the processing speed of an electrical circuits. However, any optical multicasting communication system faces a major challenge. Figure 17 illustrates examples of optical multicasting and network coding. In the typical optical multicasting network shown in Fig. 17(a), two wavelength channels are required in order to prevent the signals from colliding. The major problem that this arrangement introduces is that the maximum flow

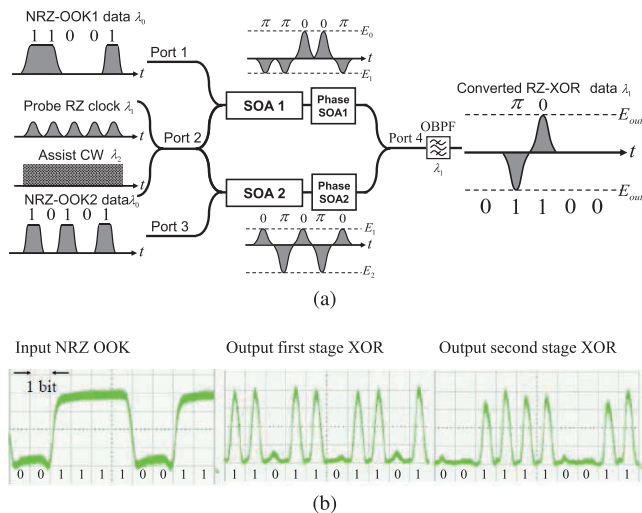


Fig. 18 XOR gate based on SOA-MZI: (a) schematic diagram and (b) input and output waveforms of XOR gates.

cannot be achieved when the multicasted signals have the same wavelength. The signal collision occurs in the system of Fig. 17 (b) when signals of the same wavelength arrive at the same relay node. To construct a more efficient optical multicasting communication system, the network coding technique has been proposed [50]. An example of network coding is shown in Fig. 17 (c). Network coding is a technique to encode signals with logical operators relating multiple signals. The exclusive or (XOR) operator can serve this purpose. Using network coding increased throughput is achieved by reducing the number of steps needed to transmit the signal. Moreover, it is possible to reduce the number of signal wavelengths needed because the signals are multiplexed within a single wavelength. Network coding also offers security advantages in that the original signal is difficult to extract from the encoded signal. However, if the optical signal is converted into an electrical signal for the encoding at the relay node, the processing speed is again limited by the electrical circuit. Therefore, all-optical network coding without optical-electrical conversion is needed [51]. All-optical network coding requires all-optical logical gates, such as XOR gate, for the encoding operations.

Figure 18 (a) shows a schematic diagram of an XOR gate using SOA-MZI [52]. NRZ-OOK signals 1 and 2 are launched into ports 1 and 3, respectively. An RZ pulse sequence is launched as a probe light into port 2. In the SOA, the refractive index is modulated because of XPM induced by the NRZ-OOK signals. The intensity of the probe light is simultaneously reduced by XGM. By properly choosing the injection current, the phase of the probe light is changed “ π ” by XPM. The output signals from SOA 1 and 2 are coupled at port 4. This coupled signal is the result of the XOR logical operation between the two channel NRZ-OOK signals. This design was used to test the feasibility of all-optical XOR gates. Figure 18 (b) shows the experimental results for a fixed input pattern in which “001111” is repeated. The NRZ-OOK 2 signal was delayed by 3 bits from NRZ-OOK

1. The data shows that the input signal of NRZ-OOK 1 and the output of the second-stage XOR are equivalent as binary data. Therefore, the cascading operation of the XOR gates as $A = B \oplus (A \oplus B)$ was successfully demonstrated. This operation includes optical decoding because the original data A was obtained from data B and data $A \oplus B$ [52]. Since the optical signal is converted to an electrical signal at the receiver end in any case, electrical decoding can also be used instead of optical decoding. The XOR gate described above can be applied for all-optical network coding.

5. Conclusions

All-optical modulation format conversion is important for the implementation of networks that adopt the different modulation formats transparently and efficiently. This article has reviewed our recent studies on modulation format conversions from OOK/BPSK and multi-channel OOK to multi-level formats using HNLf and SOA in order to show the fundamental principle and the design of the modulation format converter. In several studies, we have found that a highly functional system for OOK to multi-level modulation format conversion is possible with the serial or parallel combination of basic functional blocks. Advanced applications with WDM multicasting and network coding based OOK/BPSK converters hold great promise for elastic photonic networks to be deployed in the near future. Since the development of the modulation format for optical communication systems is still open for discussion, research on all-optical modulation format conversion will be continued.

Acknowledgments

We would like to thank Professor Ken-ichi Kitayama, The Graduate School for the Creation of New Photonics Industries, for leading this research project when he was in Osaka. This work was partially supported by Mitsubishi Electric Corporation, Japan.

References

- [1] Cisco Systems, Inc., “Cisco Visual Networking Index: Forecast and Methodology, 2016–2021,” June 2017.
- [2] P.J. Winzer and D.T. Neilson, “From Scaling Disparities to Integrated Parallelism: A Decathlon for a Decade,” *J. Lightw. Technol.*, vol.35, no.5, pp.1099–1115, March 2017.
- [3] E. Yamazaki, S. Yamanaka, Y. Kisaka, T. Nakagawa, K. Murata, E. Yoshida, T. Sakano, M. Tomizawa, Y. Miyamoto, S. Matsuoka, J. Matsui, A. Shibayama, J. Abe, Y. Nakamura, H. Noguchi, K. Fukuchi, H. Onaka, K. Fukumitsu, K. Komaki, O. Takeuchi, Y. Sakamoto, H. Nakashima, T. Mizuochi, K. Kubo, Y. Miyata, H. Nishimoto, S. Hirano, and K. Onohara, “Fast optical channel recovery in field demonstration of 100-Gbit/s Ethernet over OTN using real-time DSP,” *OSA Opt. Exp.*, vol.19, no.14, pp.13179–13184, June 2007.
- [4] H. Maeda, T. Kotanigawa, K. Saito, M. Yokota, S. Yamamoto, M. Suzuki, and T. Seki, “Field trial of simultaneous 100-Gbps and 400-Gbps transmission using advanced digital coherent technologies,” *The Optical Fiber Communication Conference (OFC2016)*, Paper W1K.4, March 2016.

- [5] IEEE P802.3bs/D2.1, Draft standard for ethernet amendment: media access control parameters, physical layers and management parameters for 200 Gb/s and 400 Gb/s, Oct. 2016.
- [6] G.N. Liu, L. Zhang, T. Zuo, and Q. Zhang, "IM/DD Transmission Techniques for Emerging 5G Fronthaul, DCI, and Metro Applications," *J. Lightw. Technol.*, vol.36, no.2, pp.560–567, Jan. 2018.
- [7] A.E. Willner, S. Khaleghi, M.R. Chitgarha, and O.F. Yilmaz, "All-Optical Signal Processing," *J. Lightw. Technol.*, vol.32, no.4, pp.660–679, Feb. 2014.
- [8] E. Ciaramella, "Wavelength Conversion and All-Optical Regeneration: Achievements and Open Issues," *J. Lightw. Technol.*, vol.21, no.11, pp.2779–2790, Nov. 2003.
- [9] O. Leclerc, B. Lavigne, E. Balmezfrezol, P. Brindel, L. Pierre, D. Rouvillain, and F. Seguinéau, "Optical Regeneration at 40 Gb/s and Beyond," *J. Lightw. Technol.*, vol.30, no.4, pp.572–582, Feb. 2012.
- [10] K.E. Stubkjaer, "Semiconductor Optical Amplifier-Based All-Optical Gates for High-Speed Optical Processing," *IEEE J. Sel. Topics Quantum Electron.*, vol.6, no.6, pp.1428–1435, Nov/Dec. 2000.
- [11] S. Oda and A. Maruta, "All-Optical Digital-to-Analog Conversion Using Nonlinear Optical Loop Mirrors," *IEEE Photon. Technol. Lett.*, vol.18, no.5, pp.703–705, March 2006.
- [12] A. Maruta and S. Oda, "All-Optical Analog-to-Digital and Digital-to-Analog Conversions Based on Fiber Nonlinearities," *International J. Microwave and Optic. Technol.*, vol.1, no.2, pp.553–558, Aug. 2006.
- [13] K. Mishina, S. Kitagawa, and A. Maruta, "All-optical modulation format conversion from on-off keying to multiple-level phase-shift-keying based on nonlinearity in optical fiber," *OSA Opt. Exp.*, vol.15, no.13, pp.8444–8453, June 2007.
- [14] K. Mishina, A. Maruta, S. Mitani, T. Miyahara, K. Ishida, K. Shimizu, T. Hatta, K. Motoshima, and K. Kitayama, "NRZ-OOK-to-RZ-BPSK modulation-format conversion using SOA-MZI wavelength converter," *J. Lightw. Technol.*, vol.24, no.10, pp.3751–3758, Oct. 2006.
- [15] A. Maruta, "Distortion-less all-optical tunable delay line based on soliton's temporal shift due to cross phase modulation in optical fiber," *The 4th International Conference on Optical Communications and Networks (ICOON2005)*, pp.131–134, Dec. 2005.
- [16] S. Inudo, Y. Yoshida, A. Maruta, and K. Kitayama, "Experimental Demonstration of Wavelength-shift-free Optical Phase Conjugation Using Orthogonal Pumps," *The 10th Conference on Lasers and Electro-Optics Pacific Rim, and the 18th OptoElectronics and Communications Conference / Photonics in Switching 2013 (CLEO-PR&OECC/PS 2013)*, Paper Th03-2, July 2013.
- [17] D. Hisano, A. Maruta, and K. Kitayama, "Synchronization Detection Using XGM in SOA for All-Optical Preprocessing," *IEEE Photon. Technol. Lett.*, vol.26, no.10, pp.1015–1018, May 2014.
- [18] A.E. Willner, B. Zhang, L. Zhang, L. Yan, and I. Fazal, "Optical Signal Processing Using Tunable Delay Elements Based on Slow Light," *IEEE J. Sel. Topics Quantum Electron.*, vol.14, no.3, pp.691–705, May/June 2008.
- [19] S. Oda, A. Maruta, and K. Kitayama, "All-Optical Quantization Scheme Based on Fiber Nonlinearity," *IEEE Photon. Technol. Lett.*, vol.16, no.2, pp.587–589, Feb. 2004.
- [20] S. Tomioka, T. Kanou, T. Kunihiro, and A. Maruta, "All-optical Non-integer Ratio Bit-rate Conversion Using Soliton Collision in Optical Fiber," *International Conference on Photonics in Switching 2009 (PS2009)*, Paper ThI1-5, Sept. 2009.
- [21] S. Oda and A. Maruta, "A Novel Quantization Scheme by Slicing Supercontinuum Spectrum for All-Optical Analog-to-Digital Conversion," *IEEE Photon. Technol. Lett.*, vol.17, no.2, pp.465–467, Feb. 2005.
- [22] A. Maruta and N. Hashimoto, "Experimental Demonstration of All-optical Modulation Format Conversion from NRZ/OOK to RZ-8APSK Based on Fiber Nonlinearity," *The Optical Fiber Communication Conference and Exposition (OFC/NFOEC 2012)*, Paper OM3B.1, March 2012.
- [23] G. Agrawal, "Nonlinear Fiber Optics," Fifth ed., Academic Press, US, Oct. 2012.
- [24] M.J. Connelly, "Semiconductor Optical Amplifiers," Kluwer Academic Publishers, Dordrecht, The Netherlands, Jan. 2002.
- [25] J. Leuthold, C. Koos, and W. Freude, "Nonlinear silicon photonics," *Nature Photon.*, vol.4, no.8, pp.535–544, Aug. 2010.
- [26] C. Langrock, S. Kumar, J.E. McGeehan, A.E. Willner, and M.M. Fejer, "All-optical signal processing using $\chi^{(2)}$ nonlinearities in guided-wave devices," *J. Lightw. Technol.*, vol.24, no.7, pp.2579–2592, July 2006.
- [27] J.C. Knight and D.V. Skryabin, "Nonlinear waveguide optics and photonic crystal fibers," *OSA Opt. Exp.*, vol.15, no.23, pp.15365–15376, Nov. 2007.
- [28] M. Sugawara, N. Hatori, T. Akiyama, Y. Nakata, and H. Ishikawa, "Quantum-Dot Semiconductor Optical Amplifiers for High Bit-Rate Signal Processing over 40 Gbit/s," *JSAP Jpn. J. Appl. Phys.*, vol.40, no.5B, pp.L488–L491, May 2001.
- [29] T. Durhuus, C. Joergensen, B. Mikkelsen, R.J.S. Pedersen, and K.E. Stubkjaer, "All-optical data wavelength conversion by SOA's in a Mach-Zehnder configuration," *IEEE Photon. Technol. Lett.*, vol.6, no.1, pp.53–55, Jan. 1994.
- [30] M. Asghari, I.H. White, and R.V. Penty, "Wavelength conversion using semiconductor optical amplifiers," *J. Lightw. Technol.*, vol.15, no.7, pp.1181–1190, July 1997.
- [31] C. Yan, Y. Su, L. Yi, L. Leng, X. Tian, X. Xu, and Y. Tian, "All-optical format conversion from NRZ to BPSK using a single saturated SOA," *IEEE Photon. Technol. Lett.*, vol.18, no.22, pp.2368–2369, Oct. 2006.
- [32] S. Arahira, H. Murai, and K. Fujii, "All-Optical Modulation-Format Converter Employing Polarization-Rotation-Type Nonlinear Optical Fiber Loop Mirror," *IEEE Photon. Technol. Lett.*, vol.20, no.18, pp.1530–1532, Sept. 2008.
- [33] Y. Lu, F. Liu, M. Qiu, and Y. Su, "All-optical format conversions from NRZ to BPSK and QPSK based on nonlinear responses in silicon microring resonators," *OSA Opt. Exp.*, vol.15, no.21, pp.14275–14282, Oct. 2007.
- [34] W. Astar, P. Apiratikul, B.M. Cannon, T. Mahmood, J.J. Wathen, J.V. Hryniewicz, S. Kanakaraju, C.J.K. Richardson, T.E. Murphy, and G.M. Carter, "Conversion of RZ-OOK to RZ-BPSK by XPM in a Passive AlGaAs Waveguide," *IEEE Photon. Technol. Lett.*, vol.23, no.19, pp.1397–1399, Oct. 2011.
- [35] H. Terauchi, A. Tokunaga, N. Horaguchi, and A. Maruta, "Design of All-Optical NRZ-OOK/RZ-QPSK Modulation Format Converter by Use of Cross Phase Modulation in Optical Fiber," *The 17th Opto-Electronics and Communications Conference (OECC2012)*, Paper 6F1-5, July 2012.
- [36] T. Miyazaki, T. Kodama, and M. Hanawa, "Demonstration of PAM4 to QPSK modulation format conversion using XPM," *IEICE Technical Report, PN2018-6*, pp.9–16, June 2018.
- [37] B. Zhang, H. Zhang, C. Yu, X. Cheng, Y.K. Yeo, P.-K. Kam, J. Yang, H. Zhang, Y.-H. Wen, and K.-M. Feng, "An All-Optical Modulation Format Conversion for 8QAM Based on FWM in HNLF," *IEEE Photon. Technol. Lett.*, vol.25, no.4, pp.327–330, Feb. 2013.
- [38] K. Mishina, S.M. Nissanka, A. Maruta, S. Mitani, K. Ishida, K. Shimizu, T. Hatta, and K. Kitayama, "All-optical modulation format conversion from NRZ-OOK to RZ-QPSK using parallel SOA-MZI OOK/BPSK converters," *OSA Opt. Exp.*, vol.15, no.12, pp.7774–7785, June 2007.
- [39] I. Kang, M.S. Rasras, L.L. Buhl, M. Dinu, G. Raybon, S. Cabot, M.A. Cappuzzo, L.T. Gomez, Y.F. Chen, S.S. Patel, A. Piccirilli, J. Jaques, and C.R. Giles, "High-Speed All-Optical Generation of Advanced Modulation Formats Using Photonic-Integrated All-Optical Format Converter," *IEEE J. Sel. Topics Quantum Electron.*, vol.18, no.2, pp.765–771, March/April 2012.
- [40] H. Kishikawa, P. Seddighian, N. Goto, S. Yanagiya, and L.R. Chen, "All-optical modulation format conversion from binary to quadrature phase-shift keying using delay line interferometer," *IEEE*

- Photonics Conference (IPC11), Paper WO2, Oct. 2011.
- [41] K. Mishina, T. Kono, A. Maruta, and K. Kitayama, "All-Optical OOK-to-16QAM Format Conversion by Using SOA-MZI Wavelength Converters," The 17th Opto-Electronics and Communications Conference (OECC2012), Paper P1-15, July 2012.
- [42] D. Hisano, A. Maruta, and K. Kitayama, "All-Optical Modulation Format Conversion from 4-channels NRZ-OOK to RZ-16QAM using SOA-MZI Wavelength Converters," IEEE Photonics Conference 2012 (IPC 2012), Paper MM3, Sept. 2012.
- [43] T. Sakamoto, A. Chiba, and T. Kawanishi, "50 Gb/s 16 QAM by a quad-parallel Mach Zehnder modulator," The 33rd European Conference and Exhibition on Optical Communication (ECOC2007), Paper PDP2.8, Sept. 2007.
- [44] G. Huang, Y. Miyoshi, A. Maruta, Y. Yoshida, and K. Kitayama, "All-Optical OOK to 16-QAM Modulation Format Conversion Employing Nonlinear Optical Loop Mirror," J. Lightw. Technol., vol.30, no.9, pp.1342–1350, May 2012.
- [45] G. Huang, Y. Miyoshi, A. Maruta, and K. Kitayama, "All-optical technique for modulation format conversion from NRZ-OOK to RZ-16QAM employing nonlinear optical loop mirror with 1:2 coupler," OSA Opt. Exp., vol.20, no.24, pp.27311–27321, Nov. 2012.
- [46] L. Rau, B.-E. Olsson, and D.J. Blumenthal, "Wavelength multicasting using an ultra high-speed all-optical wavelength converter," The Optical Fiber Communication Conference (OFC2001), Paper WDD52, March 2001.
- [47] G. Contestabile, A. Maruta, S. Sekiguchi, K. Morito, M. Sugawara, and K. Kitayama, "All-optical wavelength multicasting in a QD-SOA," IEEE J. Quantum Electron., vol.47, no.4, pp.541–547, March 2011.
- [48] D. Hisano, T. Kono, A. Maruta, N. Ohata, H. Aruga, E. Ishimura, A. Sugitatsu, and K. Kitayama, "Wavelength Multicasting Accompanied with All-Optical Modulation Format Conversion from NRZ-OOK to RZ-BPSK using SOA-MZI Wavelength Converter," The 17th Opto-Electronics and Communications Conference (OECC2012), Paper 6F1-4, July 2012.
- [49] N. Horaguchi, A. Tokunaga, and A. Maruta, "All-optical NRZ-OOK/RZ-BPSK Modulation Format Conversion for Wavelength Multicasting Based on Cross-Phase Modulation in Optical Fiber," International Conference on Photonics in Switching 2012 (PS2012), Paper Fr-S17-O19, Sept. 2012.
- [50] R. Ahlswede, N. Cai, S.-Y.R. Li, and R.W. Yeung, "Network information flow," IEEE Trans. Inf. Theory, vol.46, no.4, pp.1204–1216, July 2000.
- [51] E.D. Manley, J.S. Deogun, L. Xu, and D.R. Alexander, "All-Optical Network Coding," J. Opt. Commun. Netw., vol.2, no.4, pp.175–190, March 2010.
- [52] D. Hisano, A. Maruta, and K. Kitayama, "Demonstration of All-Optical Network Coding by using SOA-MZI based XOR Gates," The Optical Fiber Communication Conference and Exposition (OFC/NFOEC 2013), Paper JW2A.58, March 2013.



Ken Mishina received the B.E., M.E., and Ph.D. degrees in electrical, electronic, and information engineering from Osaka University, Osaka, Japan, in 2005, 2007, and 2012, respectively. In 2007, he joined Shimadzu Corporation, Kyoto, Japan. Since 2018, he has been an Associate Professor with the Department of Information and Communication Technology, the Division of Electrical, Electronic, and Information Engineering, Graduate School of Engineering, Osaka University. His current research interests include optical fiber communication systems, all-optical signal processing and photovoltaics. Dr. Mishina is a member of the IEEE Photonics Society and the Institute of Electronics, Information, and Communication Engineers (IEICE) of Japan.



Daisuke Hisano received the B.E., M.E., and Ph.D. degrees in electrical, electronic and information engineering from Osaka University, Osaka, Japan, in 2012, 2014, and 2018, respectively. In 2014, he joined NTT Access Network Service Systems Laboratories, Yokosuka, Japan. Since 2018, he has been an Assistant Professor with the Department of Information and Communication Technology, the Division of Electrical, Electronic, and Information Engineering, Graduate School of Engineering, Osaka University. His research interests include optical-wireless converged networks, optical communication, and all-optical signal processing. He is a member of the IEEE and the IEICE of Japan.



Akihiro Maruta received the B.E., M.E., and Ph.D. degrees from Osaka University, Osaka, Japan, in 1988, 1990, and 1993, respectively, all in communications engineering. He was with the Department of Communications Engineering, Osaka University, in 1993. He has been a Professor in the Department of Information and Communication Technology, Osaka University, since 2016. His current research interests include optical fiber communication systems and all-optical signal processing. Dr. Maruta is a member of the IEEE Photonics Society and the Optical Society of America.